Infrared Physics and Technology 110 (2020) 103465

Contents lists available at ScienceDirect

Infrared Physics & Technology

journal homepage: www.elsevier.com/locate/infrared

Regular article

Multiple targets inequality constrained energy minimization for multispectral imagery

Liangliang Zhu, Lei Wang, Luyan Ji, Weitun Yang, Xiurui Geng*

Aerospace Information Research Institute, Chinese Academy of Sciences, Beijing, China
Key Laboratory of Technology in Geo-Spatial information Processing and Application System, Chinese Academy of Sciences, Beijing, China
School of Electronic, Electrical and Communication Engineering, University of Chinese Academy of Sciences, Beijing, China

ARTICLE INFO

Keywords:
Multispectral imagery
Multi-targets detection
Constrained energy minimization

ABSTRACT

Multiple Targets Constrained Energy Minimization is the extension of Constrained Energy Minimization in the case that the number of targets of interest is more than one. It designs a finite-impulse response filter in such a manner that the average output energy is minimized subject to unit responses to all desired targets. However, constraining the responses of all targets to a specified value is too rigid and, in many situations, not necessary. In this paper, we have found that by simply relaxing the equality constraints in Multiple Targets Constrained Energy Minimization to inequality constraints, not only can the solution space be theoretically enlarged, but also the detection accuracy of targets can be effectively improved in practical applications. Experiments with simulated and real data demonstrate the effectiveness of the presented method.

1. Introduction

Target detection in remote sensing images has been a major research area for years. Many techniques have been developed, including the spectral angle mapping (SAM) [1], orthogonal subspace projection (OSP) [2], matched filter (MF) [3–5], constrained energy minimization (CEM) [6,7], and so on. Many successful cases have been achieved by methods based on statistics and their derivations. For example, mixture tuned matched filtering (MTMF) [8], the piecewise linear strategy of target detection (PLS) [9] and so on [10–13].

The above methods can only detect one target at a time, while in some practical applications, multiple targets need to be detected. Therefore, many multiple targets detection methods are also developed and most of them can be classified into two kinds. The first kind is based on subspace projection. This kind of method is derived from the matched subspace detector (MSD) [14], which is also known as orthogonal subspace projection (OSP). MSD and OSP calculate the length of a pixel spectrum projected in the subspace formed by the targets. There are also many variants of MSD, for example, adaptive matched subspace detector (AMSD) [15], adaptive cosine estimator (ACE) [16–18] and Simplex ACE (SACE) [19]. ACE calculates the angle between the pixel spectrum and the subspace formed by the desired signatures, while SACE calculates the angle between the pixel spectrum and the simplex formed by the desired signatures. There are also nonlinear subspace projection based methods, for example, manifold learning based target detector [20], which is based on Locally Linear Embedding (LLE) [21]. The second kind is based on statistics. Most of these methods are deri'ved from CEM, for example, target-constrained interference-minimized filter (TCIMF) [22] and multiple targets CEM (MTCEM) [23]. TCIMF constrains the desired targets to unit responses and the undesired targets to zero responses, while minimizing the average output energy. MTCEM, which only constrains all targets to unit responses, is a special case of TCIMF. However, equality constraints in TCIMF and MTCEM are too rigid, and in many situations, it is unnecessary. Therefore, some methods are proposed to overcome this drawback, for example, Sum CEM (SCEM) [23], Winner-Take-All CEM (WTACEM) [24]. SCEM designs a FIR filter for each target and adds the responses of these filters together as the final result, while WTACEM takes the maximum response as the final result. Both results of SCEM and WTACEM are obtained by combining one-target detection results, so that they can avoid optimizing under multiple equality constraints. Kernel-Based TCIMF (KTCIMF) [25] is a kernel version of TCIMF, which overcomes this drawback by projecting the data into a kernel space, so that the impact of equality constraints is relieved.

Although MTCEM and TCIMF can work in many cases, we find a depressing phenomenon that their performance will be deteriorated when more interested targets need to be detected at the same time, or when the number of bands of the image is relatively small. In these two cases, the objective functions of these two methods cannot be effectively reduced, because the solution space is greatly squeezed by their

* Corresponding author.
E-mail address: gengxr@sina.com.cn (X. Geng).

https://doi.org/10.1016/j.infrared.2020.103465
Received 26 May 2020; Accepted 12 August 2020
Available online 19 August 2020

equality constraints. Fortunately, we further find that this problem can be greatly alleviated by simply transforming the equality constraints in MTCEM and TCIMF into inequality constraints, since loosing the constraints can efficiently enlarge the solution space, where a potentially better solution can be found. In the following, we will elaborate on the effectiveness and necessity of introducing inequality constraints for MTCEM.

2. Background

In this section, CEM and its variant MTCEM are introduced. The idea of CEM arises in Minimum Variance Distortionless Response (MVDR) [26] in array processing, which constrains the desired signature by a specified gain while minimizing the filter output energy. MTCEM [23], a multiple targets extension of CEM, can detect multiple targets at a time by constraining all desired signatures to unit responses.

Assume that a spectral data $\mathbf{X} = [\boldsymbol{x}_1, \boldsymbol{x}_2, \cdots, \boldsymbol{x}_N]$ is given, where N is the number of the pixels, $\boldsymbol{x}_i$ for $1 \leqslant i \leqslant N$ is a pixel vector with length L, which is the number of the bands, and the desired signature $\boldsymbol{d}$ is known as a priori.

2.1. CEM

The CEM method designs a finite-impulse response (FIR) filter that minimizes the average output energy, while constraining the response of the target to a specific value. The whole process can be considered as a convex optimization problem subject to an equality constraint,

$$\min_{\boldsymbol{w}}\{\boldsymbol{w}^{\mathrm{T}}\mathbf{R}\boldsymbol{w}\} \quad \text{s. t.} \quad \boldsymbol{d}^{\mathrm{T}}\boldsymbol{w} = \mathbf{1}, \tag{1}$$

where $\boldsymbol{w} = [w_1, w_2, \cdots, w_L]^{\mathrm{T}}$ is the FIR filter with the length of L and $\mathbf{R} = \frac{1}{N}\mathbf{X}\mathbf{X}^{\mathrm{T}}$ represents the correlation matrix of the data. The solution is given by

$$\boldsymbol{w}_{\mathrm{CEM}} = \mathbf{R}^{-1}\boldsymbol{d}(\boldsymbol{d}^{\mathrm{T}}\mathbf{R}^{-1}\boldsymbol{d})^{-1}. \tag{2}$$

CEM can only detect one target at a time, but in many cases, we need to detect multiple targets of interest at the same time. So let's introduce an extension of CEM for multi-targets situation in the following.

2.2. MTCEM

The MTCEM method designs a FIR filter that minimizes the average output energy while constraining the responses of all targets to a specific value. Assume that $\mathbf{D} = [\boldsymbol{d}_1, \boldsymbol{d}_2, \cdots, \boldsymbol{d}_M]$ is the desired signature matrix which contains M spectra, and the constraints in MTCEM are defined by

$$\mathbf{D}^{\mathrm{T}}\boldsymbol{w} = \boldsymbol{1}, \tag{3}$$

where $\mathbf{1}$ is an M-length column vector with all elements equal to 1. Then the optimization problem can be described as

$$\min_{\boldsymbol{w}}\{\boldsymbol{w}^{\mathrm{T}}\mathbf{R}\boldsymbol{w}\} \quad \text{s. t.} \quad \mathbf{D}^{\mathrm{T}}\boldsymbol{w} = \boldsymbol{1}. \tag{4}$$

The solution is given by

$$\boldsymbol{w}_{\mathrm{MTCEM}} = \mathbf{R}^{-1}\mathbf{D}(\mathbf{D}^{\mathrm{T}}\mathbf{R}^{-1}\mathbf{D})^{-1}\boldsymbol{1}. \tag{5}$$

We find that MTCEM is severely influenced by the equality constraints, especially when the number of the desired signatures and the number of the bands are close. Usually, the average output energy is mainly determined by the background, because the target pixels account for a small portion of the entire image in general. Thus, the direction of the filter should be close to the minimum variance direction of the background. But the equality constraints greatly limit the direction of the filter, in other words, the solution space is limited (more targets, more constraints and smaller solution space). Fig. 1 shows two examples of 2-D simulated data with two targets, from which, we can find that in order to meet the equality constraints, the $\boldsymbol{w}_{\mathrm{MTCEM}}$ operator has to be perpendicular to the line connecting the two targets. Therefore, although the backgrounds of these two examples are exactly the same, the final MTCEM filter operators are quite different. This indicates that the use of equality constraints in MTCEM makes the final filter susceptible to the distribution of targets. In order to alleviate this problem, it's necessary to relax the constraints and one simple method is to change the equality constraints to inequality ones.

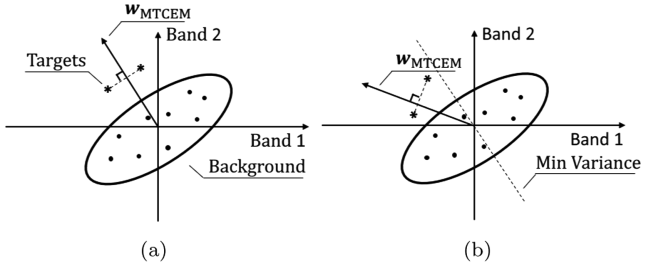

Fig. 1. 2D examples of MTCEM, the asterisks represent the targets, the dot points represent the background, the vector stands for the MTCEM filter and the dash line is the minimum variance direction of the whole data (a) targets with proper spectra (b) targets with improper spectra.

3. Method

3.1. Multiple-targets inequality constrained CEM

By investigating the shortcoming of MTCEM, which is caused by the equality constraints, we find that relaxing the constraints is a promising strategy to this problem. Therefore, the equality constraints in Fig. 3 are changed into inequality constraints, and they are redefined as

$$\mathbf{D}^{\mathrm{T}}\boldsymbol{w} \geqslant \boldsymbol{1}. \tag{6}$$

Then the optimization problem can be described as

$$\min_{\boldsymbol{w}}\{\boldsymbol{w}^{\mathrm{T}}\mathbf{R}\boldsymbol{w}\} \quad \text{s. t.} \quad \mathbf{D}^{\mathrm{T}}\boldsymbol{w} \geqslant \boldsymbol{1}. \tag{7}$$

This is a quadratic minimization problem with linear constraints, which can be solved by the Quadratic Programming (QP) [27].

3.2. The superiority of MTICEM

Comparing the constraints of MTCEM and MTICEM, it can be easily found that the solution space of MTICEM always contains the solution space of MTCEM. Therefore, the performance of MTICEM is never worse than that of MTCEM.

In addition, we also have the following lemma:

Lemma 1. *When there is only one target of interest, MTICEM and MTCEM are equivalent.*

Proof. According to the Karush-Kuhn-Tucker (KKT) conditions [28], we have: the optimal solution of an inequality constrained convex optimization problem is either on the boundary of the solution space or inside the solution space. If the optimal solution is inside the solution space, the solution is also the optimal unconstrained solution. In this problem, the optimal unconstrained solution is $\boldsymbol{w} = \boldsymbol{0}$, which doesn't meet the constraints. Therefore, the optimal solution cannot be inside the solution space and must be on the boundary. This indicates that at least one desired signature has a response of 1. Then we can come to the conclusion that when there is only one target of interest, MTICEM and MTCEM are equivalent. □

In the following, some two band examples are used to demonstrate how MTICEM works. When there is only one target of interest ($\boldsymbol{d}_1$), the MTCEM filter should meet the equality constraint

$$\boldsymbol{d}_1^{\mathrm{T}}\boldsymbol{w}_{\mathrm{MTCEM}} = 1, \tag{8}$$

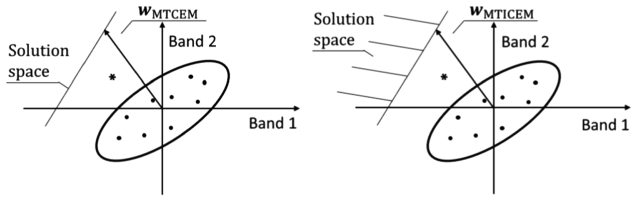

Fig. 2. Schematics of solution space with one target (in this case, the filter designed by MTICEM is the same as MTCEM) (a) the solution space of MTCEM is a line (b) the solution space of MTICEM is a half plane.

which means that in Fig. 2(a), the MTCEM filter is constrained in a straight line. On the other side, the MTICEM filter only needs to meet an inequality constraint

$$\boldsymbol{d}_1^{\mathrm{T}}\boldsymbol{w}_{\mathrm{MTICEM}} \geqslant 1, \tag{9}$$

whose solution space is the half plane in Fig. 2(b). But the optimal solution for MTICEM must be on the boundary, which is exactly the solution space of MTCEM.

If there are two targets ($\boldsymbol{d}_1$ and $\boldsymbol{d}_2$) needed to be detected at the same time, the MTCEM filter should meet two equality constraints

$$\begin{cases} \boldsymbol{d}_1^{\mathrm{T}}\boldsymbol{w}_{\mathrm{MTCEM}} = 1 \\ \boldsymbol{d}_2^{\mathrm{T}}\boldsymbol{w}_{\mathrm{MTCEM}} = 1 \end{cases}, \tag{10}$$

which means that the MTCEM filter is constrained to the intersection of two straight lines (the point labeled by a pentagram in Fig. 3(a)). Meanwhile, the MTICEM filter only needs to meet two inequality constraints

$$\begin{cases} \boldsymbol{d}_1^{\mathrm{T}}\boldsymbol{w}_{\mathrm{MTICEM}} \geqslant 1 \\ \boldsymbol{d}_2^{\mathrm{T}}\boldsymbol{w}_{\mathrm{MTICEM}} \geqslant 1 \end{cases}, \tag{11}$$

therefore, the solution space of MTICEM is the intersection of two half planes in Fig. 3(b). As can be found that the equality constraints greatly limit the solution space and the filter must be perpendicular to the line connecting the two targets. However, in this direction, not only the targets cannot be distinguished from the background well, but also the background has a large variance. While the inequality constraints in MTICEM effectively enlarge the solution space and the direction of $\boldsymbol{w}_{\mathrm{MTICEM}}$ is much closer to the minimum variance direction of the background. Though these two targets have different responses, the detection result of MTICEM is better than that of MTCEM. This demonstrates that relaxing the constraints is a simple and feasible solution for obtaining lower average output energy and better detection performance. We can also find that $\boldsymbol{w}_{\mathrm{MTICEM}}$ is on the boundary of the solution space and one of the targets has a response of 1, which is consistent with the KKT conditions.

3.3. The computational complexity of MTCEM and MTICEM

Because MTCEM only works when the number of targets is less than or equal to the number of bands, thus, in the following analysis, we assume that $M \leqslant L$. According to (5), the calculation of the MTCEM filter contains two main operations: matrix multiplication and matrix inversion, whose computational complexity is both $O(L^3)$. Therefore, the computational complexity of calculating a MTCEM filter is $O(L^3)$.

For MTICEM, a variety of methods are commonly used for the QP problem, where the most famous one is the interior point method (IPM). IPM provides a guarantee to solve optimization problems in $O(\sqrt{M}\ln(1/\epsilon))$ [29] iterations, where ϵ is the required accuracy and is usually set to 10^{-12}. Noting that within each iteration of IPM, the inverse of the hessian matrix of the objective function need to be calculated, which has the computational complexity of $O(L^3)$. Overall, the computational complexity of calculating the MTICEM filter is $O(L^3\sqrt{M}\ln(1/\epsilon))$.

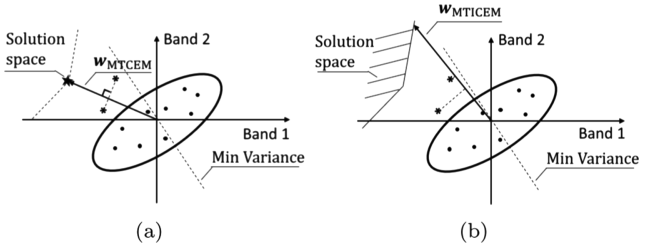

Fig. 3. Schematics of solution space with two targets (a) the solution space of MTCEM is a point (b) the solution space of MTICEM is a region.

4. Experiments

In this section, an experiment with a synthetic two band image is conducted at first to demonstrate the advantage of MTICEM. Then experiments with real images are conducted to study the relationship between the performance of MTICEM and the number of bands and the number of desired signatures. In addition, MTICEM and several multiple targets detection methods are used in the cloud detection task for comparison.

4.1. Synthetic image experiment

First, we synthesize a two band image with the size of 64×64, whose groundtruth is shown in Fig. 4(a), to intuitively show the advantage of MTICEM. The black area represents the background, which obeys the Gaussian random distribute. The red area represents target1 and the blue area represents target2, whose spectra are shown in Fig. 4(b). The detection results of MTCEM and MTICEM are shown in Fig. 5, from which we can find that the responses of the two targets in MTCEM are the same, but MTCEM does not have a good suppression on the background. On the other hand, the responses of the two targets in MTICEM are different, but the background are suppressed well. The average output energy of MTCEM (0.1973) is larger than that of MTICEM (0.1405), which further confirms our conclusion.

4.2. Salinas data set experiment

In order to investigate the relationship between the performance of MTICEM and the number of bands and the number of desired signatures, the Salinas dataset, which contains 224 spectral bands, is used to generate images of different bands (the band selection method in [30] is used). The Salinas dataset was acquired by the Reflective Optics System Imaging Spectrometer (ROSIS) sensor during a flight campaign over Pavia, northern Italy, and has 512×217 pixels. It includes 16 different classes, and the false color image and the groundtruth of this dataset are shown in Fig. 6(a) and (b).

In this experiment, class 1, 2 and 7 are chosen as the interest of targets and the groundtruth is shown in Fig. 6(c). Images with different bands are generated to investigate the relationship between the

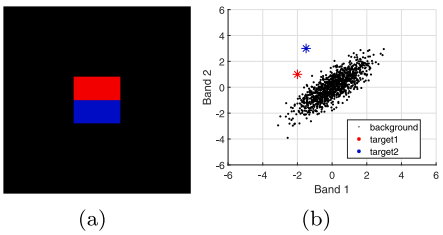

Fig. 4. (a) The groundtruth of the two band image (b) the spectra of the targets and background of the two band image.

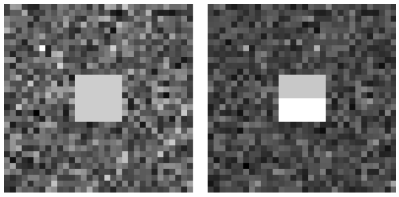

(a) (b)

Fig. 5. The detection result of the two band image (a) MTCEM: the average output energy is 0.1973 (b) MTICEM: the average output energy is 0.1405.

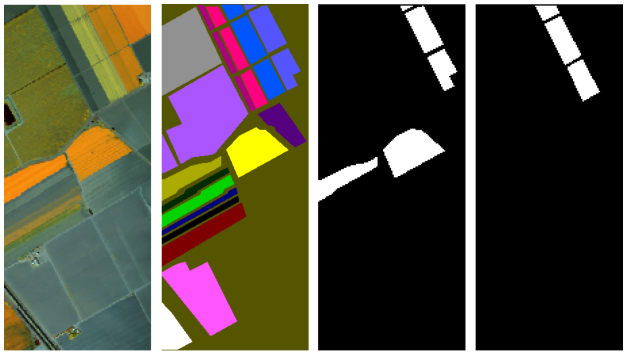

(a) (b) (c) (d)

Fig. 6. The Salinas dataset: (a) false color image (R: band 50, G: band 100, B: band 200) (b) groundtruth (c) the groundtruth of class 1, 2, and 7 (d) the groundtruth of class 6.

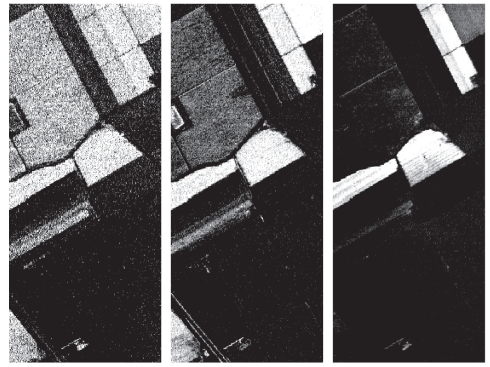

(a) 10 bands (b) 30 bands (c) 50 bands

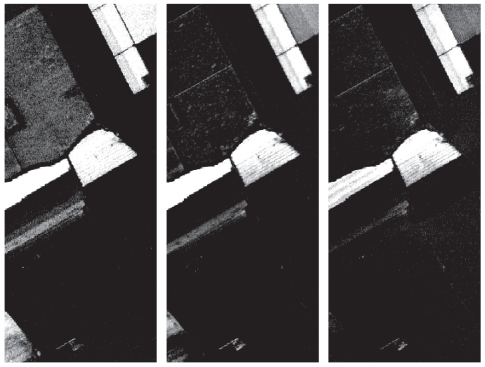

(d) 10 bands (e) 30 bands (f) 50 bands

Fig. 7. Detection results for the Salinas dataset with different bands (a-c) MTCEM (d-f) MTICEM.

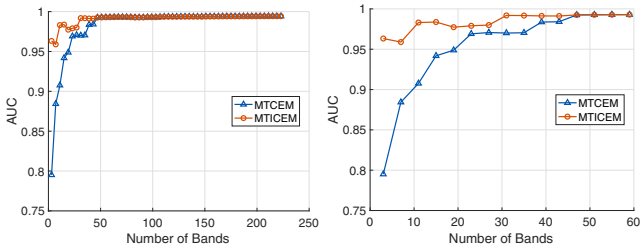

(a) (b)

Fig. 8. The AUC (area under the receiver operating characteristic curve) curves for the Salinas dataset with different bands (a) the number of bands ranges from 3 to 224 (b) the number of bands ranges from 3 to 59 (a partial enlarged view of (a)).

performance of MTICEM and the number of bands. The three mean spectra of three targets are used as the desired signatures of MTCEM and MTICEM. From Fig. 8(a), we can find that though the performance of MTCEM gradually catches up with that of MTICEM, MTICEM is never worse than MTCEM. When the number of bands is large, the solution space of MTCEM is large enough to find a good solution, thus, MTCEM and MTICEM have almost the same performance in this case. It can also be seen from Fig. 8(b) that MTICEM is much more superior than MTCEM, when the number of bands is small. From Fig. 7(a), it can be found that when there are only a few bands, MTCEM is heavily suffered from the equality constraints, which leads to an insufficient suppression on the background. Meanwhile, the detection results of MTICEM shown in Fig. 7(d)–(f) are relative stable and the targets are well detected. Noting that MTICEM has a more obvious advantage when the number of bands is small, thus MTICEM is recommended for multispectral images.

In practice, there is another situation, where multiple desired signatures are needed to be detected. Due to the spatial variability, the spectra of the same target may be different. In this case, using multiple spectra of the same target as the desire signatures can improve the detection performance to some extent. In this experiment, the 6th class is selected as the target, whose groundtruth is shown in Fig. 6(d), and 30 bands are selected from the Salinas data set. Because the desired signatures are randomly selected from the image, Fig. 10 is the mean result of 50 runs. We can find from Fig. 9(b) that when more spectra of the target are involved, MTCEM can obtain a better performance. However, when we continue adding spectra to the desired signatures, the performance of MTCEM will rapidly drop, which can be seen from Fig. 9(a). The reason for this phenomenon is still that too many equality constraints make MTCEM unable to fully consider the influence of the background. On the contrary, from Fig. 10, it can be found that the performance of MTICEM continues increasing, as there are more spectra included in the desired signatures.

4.3. Cloud detection experiment

Cloud detection is an essential and important process in satellite remote sensing. In many methods [31], the cloud probability map should be obtained at first, which has a great influence on the final detection result. However, cloud has various forms, which is hard to be detected completely by single target detecting methods. Thus, multi-targets detection methods are used in cloud detection for better performance. In this section, the used multispectral image, which has a size of 256 × 256, comes from the Landsat 8 Operational Land Imager (OLI) Thermal Infrared Sensor (TIRS) terrain corrected (Level-1T) scenes. The image consists of nine spectral bands with a spatial resolution of 30 meters for bands 1 to 7 and 9. The spatial resolution for band 8 (panchromatic) is 15 meters and the thermal bands 10 and 11 have the spatial resolution of 100 meters. Before using the dataset, all bands are resampled to the spatial resolution of 30 meters. The false color image

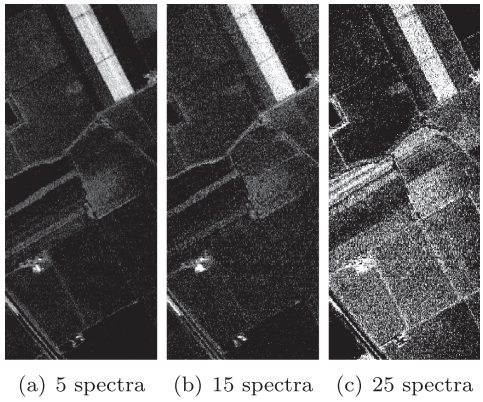

(a) 5 spectra (b) 15 spectra (c) 25 spectra

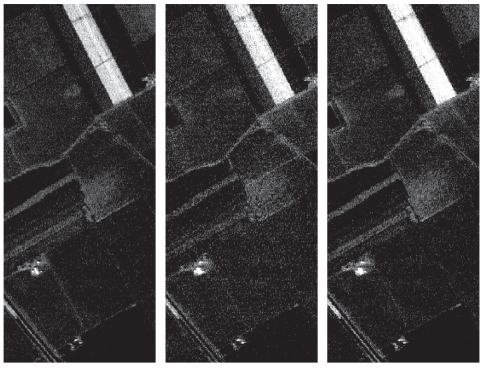

(d) 5 spectra (e) 15 spectra (f) 25 spectra

Fig. 9. Detection results for the Salinas dataset with different number of target spectra selected (a-c) MTCEM (d-f) MTICEM.

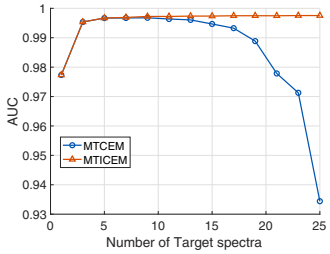

Fig. 10. The AUC curves for the Salinas dataset with different number of target spectra selected.

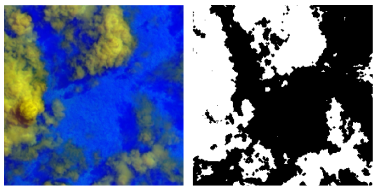

(a) (b)

Fig. 11. The sub-image from Landsat 8 level-1 data (a) false color image (R: band 1, G: band 5, B: band 10) (b) cloud mask (white: cloud, black: non-cloud). (For interpretation of the references to color in this figure legend, the reader is referred to the web version of this article.)

and the cloud mask generated by [32] are shown in Fig. 11.

To demonstrate the advantages of our method, SCEM, MTCEM, KTCIMF, and ACE are conducted for comparison. Noting that for KTCIMF, a (number of pixels) × (number of pixels) size matrix needs to be generated, which is hard in practice. Therefore, we randomly choose 1000 pixels from the image, and project all pixels including the desired

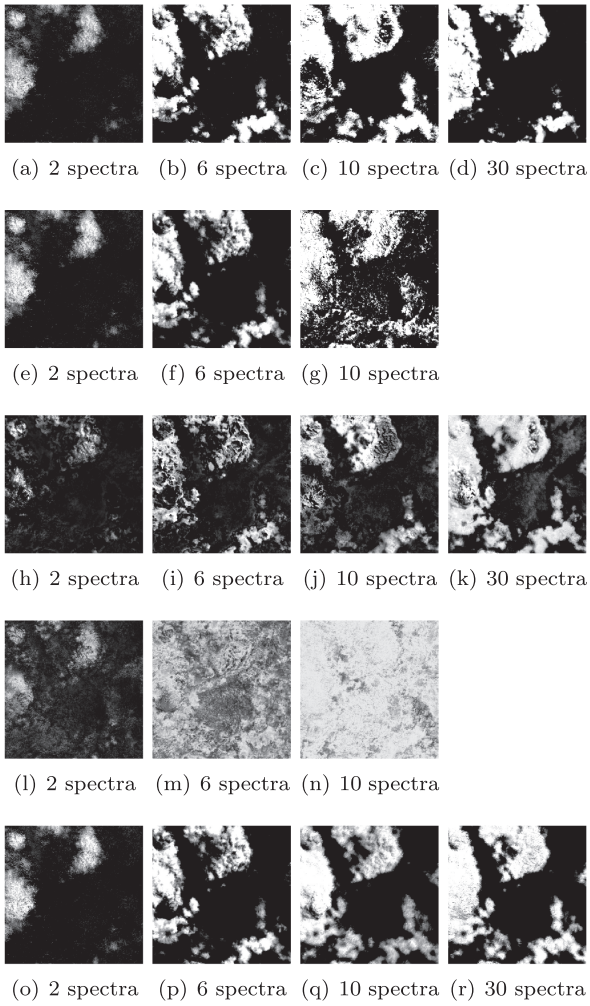

(a) 2 spectra (b) 6 spectra (c) 10 spectra (d) 30 spectra

(e) 2 spectra (f) 6 spectra (g) 10 spectra

(h) 2 spectra (i) 6 spectra (j) 10 spectra (k) 30 spectra

(l) 2 spectra (m) 6 spectra (n) 10 spectra

(o) 2 spectra (p) 6 spectra (q) 10 spectra (r) 30 spectra

Fig. 12. Cloud detection results with different number of target spectra selected (It should be noted that the number of desired signatures of MTCEM and ACE cannot be more than the number of bands, thus their results for 30 spectra selected are not compared.) (a-d) SCEM (e-g) MTCEM (h-k) KTCIMF (l-n) ACE (o-r) MTICEM.

signatures to these 1000 pixels with a Gaussian kernel of $\sigma = 4$ to approach the result of full size KTCIMF. After projecting the original data to the kernel space, the MTCEM method is performed on the projected data. The desired signatures are randomly selected from the cloud area, therefore, the detection results are the results of one run, while in order to obtain statistical results, the AUC indices are the mean of 50 runs.

From Figs. 12(a), (e), (h), (l), and (e), we can find that when only two spectra of the cloud are selected as the desired signatures, all methods can only detect part of the cloud. And from Fig. 1, we can also find that in this case, the performance of MTCEM and MTICEM are exactly the same. When more spectra of the cloud are involved, all methods have better detection results. It should be noted that ACE is a method designed for hyperspectral images, where the subspace formed by the desired signatures is small comparing the whole space. However, in multispectral images, the subspace formed by the desired signatures is relatively large, which leads to a high response for every pixel. When the number of the involved desired signatures is close to the number of bands, the performance of MTCEM and ACE begins to drop in Fig. 12(g) and (n). While the performance of SCEM, KTCIMF and MTICEM keeps increasing in Fig. 12. SCEM adds the detection results of CEM for all desired signatures together as the final result, which means that it doesn't fully consider the relationships between the desired signatures. Thus it cannot obtain the theoretically best result, and we can find from

Table 1
AUC vs the number of selected target spectra for the cloud detection results.

The number of selected spectra	SCEM	MTCEM	KTCIMF	ACE	**MTICEM**
2	0.7353	**0.7376**	0.6101	0.6111	**0.7376**
6	0.8754	0.8954	0.7533	0.6976	**0.9022**
10	0.9015	0.8615	0.8040	0.6328	**0.9389**
30[a]	0.9502	–	0.9562	–	**0.9807**

[a] It should be noted that the number of desired signatures of MTCEM and ACE cannot be more than the number of bands, thus their results for 30 spectra selected are not compared.

Fig. 1 that when only 2 or 6 target spectra are selected, the performance of SCEM is worse than MTCEM and MTICEM. KTCIMF tries to find a hyperplane in the kernel space, which corresponds to a hypersurface in the original space, to distinguish between the targets and the background. Therefore, it can efficiently suppress the background, but at the same time, due to the spatial variability of the spectra, some targets are also suppressed. This is why the AUC indices of KTCIMF are relatively small in Fig. 1. Noting that the number of desired signatures of MTCEM and ACE cannot be more than the number of bands, which limits their performance to being further improved. While SCEM, KTCIMF and MTICEM can detect the cloud better when more and more desired signatures are selected (we assume that the desired signatures only contain the spectra of the target), which can be seen from Fig. 12(d), (k) and (r). We can also find from Table 1 that MTICEM always have the largest AUC index, and it's performance can be greatly improved when 30 spectra of the cloud are involved.

5. Conclusion

The performance of MTCEM is restricted by the equality constraints. But inequality constraints can effectively expand the solution space, which makes it possible to further reduce the average output energy and improve the detection performance. Therefore, in this paper, we propose the Multiple Targets Inequality Constrained Energy Minimization (MTICEM) method to overcome the drawback of MTCEM. We compare its performance to MTCEM and some other multiple targets detection methods and find that, in the following situations, MTICEM is suggested to be used: (1) dealing with multispectral images, (2) the number of desired signatures is large.

It should be noted that, in theory, MTICEM is never worse than MTCEM. Thus, if real-time processing is unnecessary, using MTICEM instead of MTCEM is recommended.

Declaration of Competing Interest

The authors declare that they have no known competing financial interests or personal relationships that could have appeared to influence the work reported in this paper.

References

[1] S. Narumalani, D.R. Mishra, J. Burkholder, P.B. Merani, G. Willson, A comparative evaluation of isodata and spectral angle mapping for the detection of saltcedar using airborne hyperspectral imagery, Geocarto Int. 21 (2) (2006) 59–66, https://doi.org/10.1080/10106040608542384.

[2] J.C. Harsanyi, C. Chang, Hyperspectral image classification and dimensionality reduction: an orthogonal subspace projection approach, IEEE Trans. Geosci. Remote Sens. 32 (4) (1994) 779–785, https://doi.org/10.1109/36.298007.

[3] D. Manolakis, G. Shaw, Detection algorithms for hyperspectral imaging applications, IEEE Signal Process. Mag. 19 (1) (2002) 29–43, https://doi.org/10.1109/79.974724.

[4] D.G. Manolakis, R.B. Lockwood, T.W. Cooley, J. Jacobson, Is there a best hyperspectral detection algorithm, vol. 7334, 2009. doi:10.1117/12.816917.

[5] D. Manolakis, R. Lockwood, T. Cooley, J. Jacobson, Hyperspectral detection algorithms: use covariances or subspaces, vol. 7457, 2009. doi:10.1117/12.828397.

[6] J. Harsanyi, W. Farrand, C.-I. Chang, Detection of subpixel spectral signatures in hyperspectral image sequences, in: Annual Meeting, Proceedings of American Society of Photogrammetry and Remote Sensing, 1994, pp. 236–247.

[7] W.H. Farrand, J.C. Harsanyi, Mapping the distribution of mine tailings in the Coeur d'Alene river Valley, Idaho, through the use of a constrained energy minimization technique, Remote Sens. Environ. 59 (1) (1997) 64–76, https://doi.org/10.1016/S0034-4257(96)00080-6 http://www.sciencedirect.com/science/article/pii/S0034425796000806.

[8] J.J. Mitchell, N.F. Glenn, Subpixel abundance estimates in mixture-tuned matched filtering classifications of leafy spurge (Euphorbia esula L.), Int. J. Remote Sens. 30(23) (2009) 6099–6119. arXiv:https://doi.org/10.1080/01431160902810620.

[9] X. Geng, W. Yang, L. Ji, C. Ling, S. Yang, A piecewise linear strategy of target detection for multispectral/hyperspectral image, IEEE J. Sel. Top. Appl. Earth Observ. Remote Sens. 11 (3) (2018) 951–961, https://doi.org/10.1109/JSTARS.2018.2791920.

[10] X. Geng, L. Ji, K. Sun, Clever eye algorithm for target detection of remote sensing imagery, ISPRS J. Photogramm. Remote Sens. 114 (2016) 32–39, https://doi.org/10.1016/j.isprsjprs.2015.10.014 http://www.sciencedirect.com/science/article/pii/S0924271616000216.

[11] C.A. Shah, M.K. Arora, S.A. Robila, P.K. Varshney, Ica mixture model based unsupervised classification of hyperspectral imagery, in: Applied Imagery Pattern Recognition Workshop, 2002. Proceedings., 2002, pp. 29–35. doi:10.1109/AIPR.2002.1182251.

[12] R. DiPietro, D. Manolakis, R. Lockwood, T. Cooley, J. Jacobson, Hyperspectral matched filter with false-alarm mitigation, Opt. Eng. 51 (2012) 6202, https://doi.org/10.1117/1.OE.51.1.016202.

[13] S. Jay, M. Guillaume, J. Blanc-Talon, Underwater target detection with hyperspectral data: Solutions for both known and unknown water quality, IEEE J. Sel. Top. Appl. Earth Observ. Remote Sens. 5 (4) (2012) 1213–1221, https://doi.org/10.1109/JSTARS.2012.2185488.

[14] L.L. Scharf, B. Friedlander, Matched subspace detectors, IEEE Trans. Signal Process. 42 (8) (1994) 2146–2157, https://doi.org/10.1109/78.301849.

[15] B. Thai, G. Healey, Invariant subpixel material detection in hyperspectral imagery, IEEE Trans. Geosci. Remote Sens. 40 (3) (2002) 599–608, https://doi.org/10.1109/TGRS.2002.1000320.

[16] L.L. Scharf, L.T. McWhorter, Adaptive matched subspace detectors and adaptive coherence estimators, in: Conference Record of The Thirtieth Asilomar Conference on Signals, Systems and Computers, vol 2, 1996, pp. 1114–1117. doi:10.1109/ACSSC.1996.599116.

[17] S. Kraut, L.L. Scharf, R.W. Butler, The adaptive coherence estimator: a uniformly most-powerful-invariant adaptive detection statistic, IEEE Trans. Signal Process. 53 (2) (2005) 427–438, https://doi.org/10.1109/TSP.2004.840823.

[18] A.K. Ziemann, Local spectral unmixing for target detection, 2016 IEEE Southwest Symposium on Image Analysis and Interpretation (SSIAI), 2016, pp. 77–80, , https://doi.org/10.1109/SSIAI.2016.7459179.

[19] J.T. Amanda Ziemann, Simplex ace: a constrained subspace detector, Opt. Eng. 56 (8) (2017), https://doi.org/10.1117/1.OE.56.8.081808 1 – 13 – 13.

[20] A. Ziemann, J. Theiler, D. Messinger, Hyperspectral target detection using manifold learning and multiple target spectra, 2015. doi:10.1109/AIPR.2015.7444547.

[21] S.T. Roweis, L.K. Saul, Nonlinear dimensionality reduction by locally linear embedding, Science 290 (5500) (2000) 2323–2326, https://doi.org/10.1126/science.290.5500.2323 https://science.sciencemag.org/content/290/5500/2323.full.pdf , https://science.sciencemag.org/content/290/5500/2323 ..

[22] C.-I.C. Hsuan Ren, Target-constrained interference-minimized approach to subpixel target detection for hyperspectral images, Opt. Eng. 39 (12) (2000) 3138–3145 – 8, https://doi.org/10.1117/1.1327499.

[23] H. Ren, Q. Du, C.-I. Chang, J.O. Jensen, Comparison between constrained energy minimization based approaches for hyperspectral imagery, in: IEEE Workshop on Advances in Techniques for Analysis of Remotely Sensed Data, 2003, 2003, pp. 244–248. doi:10.1109/WARSD.2003.1295199.

[24] C.-I. Chang, Hyperspectral Imaging: Techniques for Spectral Detection and Classification, Plenum Publishing Co., 2003.

[25] T. Wang, B. Du, L. Zhang, A kernel-based target-constrained interference-minimized filter for hyperspectral sub-pixel target detection, IEEE J. Sel. Top. Appl. Earth Observ. Remote Sens. 6 (2) (2013) 626–637, https://doi.org/10.1109/JSTARS.2013.2251863.

[26] M.N. Murthi, B.D. Rao, Minimum variance distortionless response (mvdr) modeling of voiced speech, in: 1997 IEEE International Conference on Acoustics, Speech, and Signal Processing, vol. 3, 1997, pp. 1687–1690. doi:10.1109/ICASSP.1997.598838.

[27] Z. Dostl, Optimal Quadratic Programming Algorithms: With Applications to Variational Inequalities, first ed., Springer Publishing Company Incorporated, 2009.

[28] W. Karush, Minima of functions of several variables with inequalities as side constraints, Master's thesis. doi:10.1007/978-3-0348-0439-4_10.

[29] J. Gondzio, Interior point methods 25 years later, Eur. J. Oper. Res. 218 (3) (2012) 587–601, https://doi.org/10.1016/j.ejor.2011.09.017.

[30] X. Geng, K. Sun, L. Ji, Y. Zhao, A fast volume-gradient-based band selection method for hyperspectral image, IEEE Trans. Geosci. Remote Sens. 52 (11) (2014) 7111–7119.

[31] S. Mahajan, B. Fataniya, Cloud detection methodologies: variants and development—a review, Complex Intell. Syst. doi:10.1007/s40747-019-00128-0.

[32] S. Foga, P.L. Scaramuzza, S. Guo, Z. Zhu, R.D. Dilley, T. Beckmann, G.L. Schmidt, J.L. Dwyer, M. Joseph Hughes, B. Laue, Cloud detection algorithm comparison and validation for operational Landsat data products, Remote Sens. Environ. 194 (2017) 379–390, https://doi.org/10.1016/j.rse.2017.03.026.